2024 IEEE Conference on Computational Imaging Using Synthetic Apertures (CISA) | 979-8-3503-0864-8/24/$31.00 ©2024 IEEE | DOI: 10.1109/CISA60639.2024.10576262

TOWARDS FULL FIELD-OF-VIEW FOURIER PTYCHOGRAPHY FOR EXTREME ULTRAVIOLET MICROSCOPE

Chaoying Gu[1], *Antoine Islegen-Wojdyla*[2], *Markus Benk*[2], *Kenneth A. Goldberg*[2], *Laura Waller*[1]

[1]University of California, Berkeley; Berkeley, CA (USA)
[1]Lawrence Berkeley National Laboratory; Berkeley, CA (USA)

ABSTRACT

We evaluate various Fourier ptychographic microscopy (FPM) reconstruction algorithms using both simulated and experimental data acquired from an Extreme Ultraviolet (EUV, 13.5 nm wavelength) microscope. We specifically focus on the algorithms' ability to robustly address field-dependent aberrations, which enables increased spatial resolution and quantitative phase imaging across an expanded field of view. We systematically compare the algorithms' performance under aberrations for a single zoneplate imaging system, utilizing Fourier Ring Correlation (FRC) as a systematic metric for assessing reconstruction quality. Furthermore, we explore the impact of systematic errors on the reconstruction of experimental data, aiming to increase the effective field of view by 25-fold, from the nominal 5x5 um^2 diffraction-limited area. Additionally, our evaluation incorporates innovative FPM-adjacent methodologies, including the Angular Ptychographic Imaging with Closed-form method (APIC), for reconstructing EUV images.

***Index Terms*—** Fourier Ptychography, Extreme ultraviolet lithography, Aperture synthesis, Full-field imaging, Aberration reconstruction, Fresnel zoneplates, X-ray, Computational imaging

1. INTRODUCTION

The quality of imaging systems is significantly influenced by their lenses, which impact various aspects such as light efficiency, resolution, and aberration. These constraints, however, can be addressed through a technique known as aperture synthesis, commonly utilized in fields like radar, astronomy, and more recently applied to microscopy.

Fourier ptychographic microscopy (FPM) [1] is a computational imaging technique that synthesizes multiple full-field images acquired with a coherent illumination with different illumination angles. This technique exploits information redundancy from overlapped spectrum to retrieve the phase and thus synthesize the complex spectrum of the object. This synthetic spectrum allows for enhanced resolution of the imaging system beyond the inherent limitations imposed by the numerical aperture of the objective lens, while also facilitating quantitative phase imaging.

The scope of FPM has expanded to include other wavelengths, such as Extreme Ultraviolet (EUV, 13.5 nm wavelength), where commercial optics are less available. In this domain, FPM has achieved a resolution of 26 nm within a central, 5x5 μm^2 diffraction-limited area [2]. However, this imaging system (the SHARP EUV microscope [3], at the Lawrence Berkeley National Laboratory), employs a single-element zoneplate objective. This configuration introduces significant aberrations beyond the sweetspot field of view (FOV), a notable limitation documented in the literature [4]. Although current algorithms are capable of concurrently reconstructing both the complex object and the pupil, they exhibit a high sensitivity to initial conditions. Consequently, existing demonstrations of FPM in the EUV spectrum have been confined to regions with minimal aberration—the 5x5 μm^2 'sweet spot' [2].

Our research aims to extend the application of FPM across a broader FOV within the EUV spectrum, computationally addressing challenges posed by limitations in optical manufacturing. We conduct a thorough aberration tolerance analysis utilizing various measurement schemes and reconstruction algorithms, incorporating prior knowledge of the aberrations wherever feasible. This approach is expected to facilitate faster imaging processes, which benefits tasks such as defect inspection, or allow the use of lower numerical aperture (NA) settings when examining sensitive samples.

2. RELATED WORK

2.1. EUV microscope characterization

We use the method and corresponding data from a previous study [4] to characterize the aberration of the EUV imaging system. The FOV is fundamentally limited by the field of the off-axis zone plate, which serves as the objective lens. We apply the aberration in the top-left corner of FoV in simulation. The RMS of the pupil function phase is 0.52π. The ground truth aberration is shown in the bottom right corner of Fig. 1 ground truth.

Authorized licensed use limited to: Lawrence Berkeley National Laboratory. Downloaded on January 14,2025 at 19:04:13 UTC from IEEE Xplore. Restrictions apply.

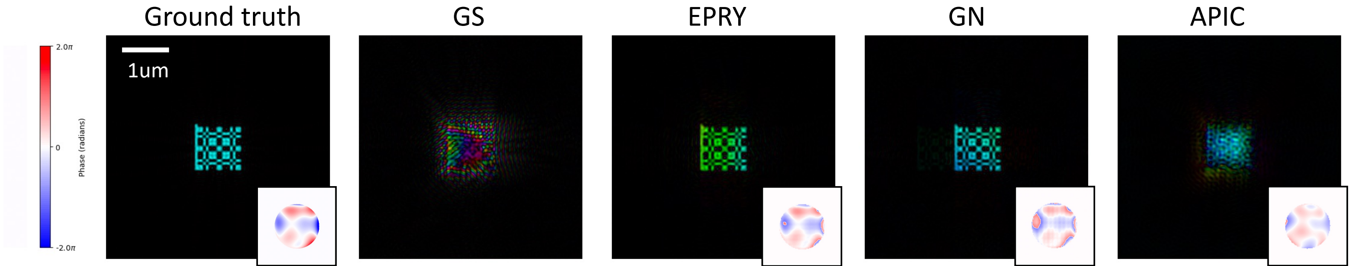

Fig. 1. Simulation of FPM reconstructions of a sub-resolution binary pseudo-random pattern under aberration using various algorithms: Gerchberg-Saxton (GS) [1], Embedded Pupil Function Recovery (EPRY) [5], Second order Gauss-Newton (GN) [6], and Angular ptychographic imaging with closed-form method (APIC) [7]. The insert shows the local reconstruction the field-varying aberrations.

2.2. Full FOV FPM

The standard way to perform full FoV FPM and account for shift-variant pupil function is to divide the FoV into patches and reconstruct separately. Ou [5] first demonstrated the full-field FoV by dividing the whole FoV into patches. Song [8] proposes a better pupil reconstruction method by using Zernike decomposition, thus achieving the full-field FPM reconstruction in the visible band.

3. SIMULATION ANALYSIS

In our simulations, we use an array of binary pseudo-random patterns, which have a relatively flat spectrum and closely approximate the characteristics of lithography masks intended for imaging. We evaluate the performance of four distinct algorithms: the First order Gerchberg-Saxton (GS) [1], Embedded Pupil Function Recovery (EPRY) [5], Second order Gauss-Newton (GN) [6], and Angular ptychographic imaging with closed-form method (APIC) [7].

The GS algorithm is applied to reconstruct images without aberration or when a ground truth aberration is provided, without solving for the aberration itself. Conversely, EPRY estimates both the object and the pupil function simultaneously, though it exhibits slow convergence, yet faithfully reconstructs the aberration. Previous survey study by Yeh et al. [9] has concluded that the GN method, with its pupil estimation capability, typically offers superior results in the presence of aberrations. However, our simulations reveal that under strong aberration conditions and specific illumination patterns, GN does not consistently outperform EPRY after full convergence. Notably, GN's main advantages are its robustness to systematic errors and rapid convergence.

APIC, a recently proposed method, aims to analytically produce robust and fast FPM reconstructions [7]. Nonetheless, it faces significant challenges in the EUV measurement context. First, while traditional FPM typically involves absorptive objects with strong DC components—a prerequisite for APIC's algorithm derivation—the EUV experiments often involve reflective objects with insufficiently strong DC components, contradicting APIC's theoretical requirements. Second, APIC demands precise NA-matching data that aligns closely with the transition between bright-field and dark-field imaging. Its performance declines when the tolerance is increased to accommodate the illumination pattern we employed in the EUV microscope.

4. EXPERIMENT EVALUATION

We use experimental data acquired from the SHARP EUV microscope. The object under investigation is a 5×5 array of binary pseudo-random patterns, well-suited for validating full FOV aberration characterization. While no higher NA lens is available in the EUV spectrum to provide a ground truth comparison—as is possible in the visible spectrum—the correlation between the reconstructions of the center and corner patches allows for a quantitative performance assessment using FRC.

The zoneplate used in our experiments has an effective NA of 0.082 designed to emulate the image formation in a 0.33 NA EUV photolithography scanner with a 4x demagnification. The theoretical diffraction limit is therefore calculated as $\lambda/2\mathrm{NA}$ = 82 nm. Each individual pattern in the array measures 1.14 µm per side with a line width of 60 nm, which exceeds this diffraction limit, indicating that the individual lines are not supposed to be well resolved in the raw measurement.

From the initial low-NA captures, as depicted in the second column of Fig. 2 (a), it is evident that: 1. the lines within even the central 'sweet spot' region are diffraction-limited, necessitating the use of synthetic aperture techniques enabled by FPM to enhance resolution; 2. the corner patches are subject to severe degradation due to aberrations, necessitating computational correction. After our implementation of full FOV FPM reconstruction, both challenges are addressed as the last column of Fig. 2 (a) displays: the previously unresolved lines become clearly defined, and the aberrations are effectively deconvolved computationally. In addition, the field-dependent pupil reconstruction in Fig. 2 (b) qualitatively matches the aberration characterization using speckle

Authorized licensed use limited to: Lawrence Berkeley National Laboratory. Downloaded on January 14,2025 at 19:04:13 UTC from IEEE Xplore. Restrictions apply.

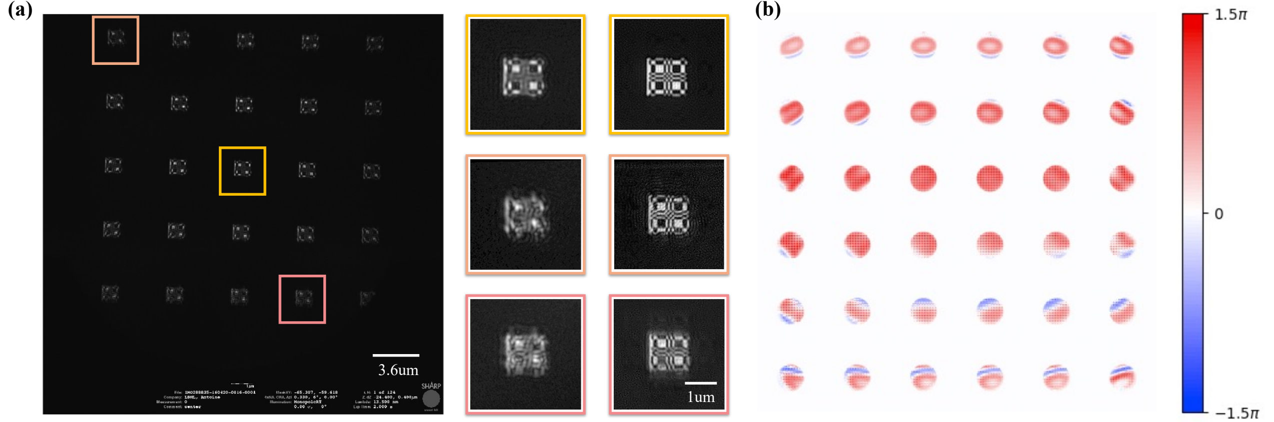

Fig. 2. Full FoV FPM reconstruction from data collected at 13.5 nm wavelength EUV microscope. (a) The raw capture in the first column with three color-coded regions highlighted for detailed analysis; the two columns to the right presents the zoomed-in raw measurements and corresponding FPM reconstructions respectively. (b) The full FoV aberration visualization, where the FoV is segmented into a 6x6 grid with 20% overlap; this grid layout shows the pupil reconstruction for each patch.

imaging in the literature [4]. In the following sections, we use Fourier ring correlation (FRC) [10] to quantitatively describe the resolution enhancement and aberration correction, and also to compare different available algorithms' reconstruction. FRC is a quantitative measure of similarity between two images in the frequency domain, expressed as a function of spatial frequency. The FRC plots provide a detailed analysis of how different frequency components contribute to the overall image reconstruction quality. It is defined by the following equation:

$$\mathrm{FRC}(R) = \frac{\widetilde{I}_1(R) \cdot \widetilde{I}_2(R)^*}{\sqrt{\left|\widetilde{I}_1(R)\right|^2 \cdot \left|\widetilde{I}_2(R)\right|^2}} \tag{1}$$

where R represents a specific spatial frequency within radius R in the frequency domain, and $\widetilde{I}_1(R)$ and $\widetilde{I}_2(R)$ are the Fourier transforms of two images extracted at radius R and treated as a 1D vector, and * denotes the complex conjugate.

4.1. Resolution enhancement

The blue envelope in Fig. 3 shows the FRC between all possible pairs between 61 central illumination calibration images, taken periodically between tilted illumination measurements to monitor any sample drift. There is a noticeable drop in the FRC at frequencies near the diffraction limit, marked by a red vertical line, indicating the fundamental physical limit. The red curve shows the FRC between two FPM reconstructions using the GN algorithm. This curve demonstrates a noticeable improvement in mid-frequency resolution, reaching closer to the limit defined by the synthetic aperture, marked by the blue vertical line. We focus on the central 332 px×332 px region out of the total 2048 px×2048 px FOV in this section to emphasize the best resolution enhancement capability of FPM. The corner regions are subject to residual aberration and the other systematic error like field-dependent wavefront tilt caused by the relative defocus between the illumination and the object plane.

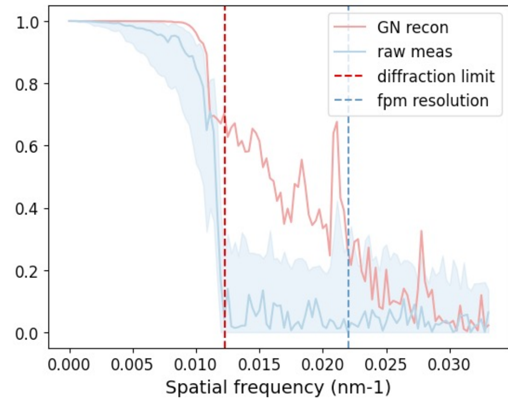

Fig. 3. FRC analysis of calibration and reconstruction images: The blue curve shows FRC across calibration images, revealing a resolution decline at the diffraction limit (red line). The red curve illustrates improved resolution in FPM reconstructions with the GN algorithm, approaching the synthetic aperture limit (blue line).

4.2. Algorithm comparison

Fig. 4 presents the reconstruction performance of various algorithms on both central and corner patches. The reconstruction from the central patch using the GN algorithm serves as a 'ground truth' to assess the effectiveness of aberration correction in other reconstructions. Ideally, the reconstruction of the corner patch should match the central patch. Fig. 4 (b) demonstrates the FRC between different algorithms' reconstructions and the 'ground truth', clearly indicating that GN

Authorized licensed use limited to: Lawrence Berkeley National Laboratory. Downloaded on January 14,2025 at 19:04:13 UTC from IEEE Xplore. Restrictions apply.

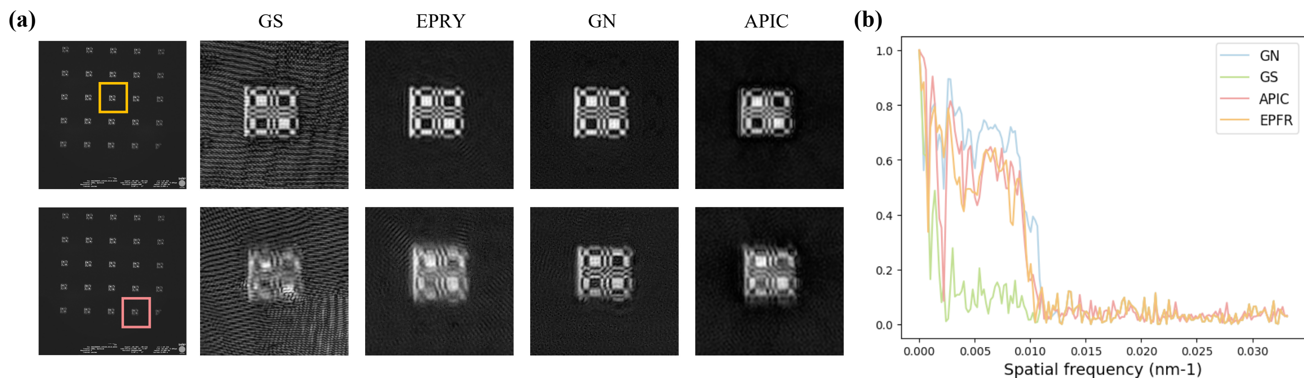

Fig. 4. (a) Each row presents a reconstruction set of a specific patch in the FoV. The first column illustrates the location of the patch in the entire raw capture, and the subsequent columns are the FPM reconstruction results using various algorithms. (b) The FRC curve between the reconstructions of the corner patch by different algorithms (as depicted in the bottom row of panel a) and the highest quality central patch reconstruction (specifically, the GN result in the top row of panel a).

achieves the highest quality of reconstruction under strong aberration. As an implementation detail, we employ Sum of Squared Differences (SSD) to register the two patches, accommodating any potentially different spacing across the FOV.

By calculating FRC between the central patch and different algorithms, we can see that GS which does not account for aberration is the worst. APIC and EPRY generates similar results, and GN is the best. For the central patch, with mild aberration, all the algorithms are doing ok. For the more challenging corner patch, GN is reconstructing the object most robustly. Note that APIC uses only 15 approximately NA-matching measurements only (opposed to 61 used by the other iterative algorithms), and it's analytical so it takes only 1s to compute, which is hundreds times faster than the other iterative algorithms. Despite the theoritical constraint specific to EUV imaging as mentioned in Sec. 3, APIC has special advantages and might be of interest for future experiments and studies.

Fig. 4 (a) visually demonstrates that both APIC and EPRY yield similar outcomes, whereas GN excels, particularly with the more challenging corner patch. However, we note that APIC operates with only 15 approximately NA-matching measurements—significantly fewer than the 61 used by other iterative algorithms—and its analytical nature allows for computation within 1 second, hundreds times faster than the other methods. Despite theoretical constraints specific to EUV imaging as discussed in Sec. 3, APIC's unique advantages make it a promising candidate for further research and experiments.

4.3. Systematic error correction

A common systematic error in visible band FPM is the misalignment of LED positions, which provide varied illumination angles. Unlike traditional systems that use LEDs, the SHARP system employs an angle scanner and a condenser to achieve tilted illumination. Therefore, in addition to potential angle calibration errors for the center patch, it is also susceptible to other field-dependent systematic errors. Previous experiments on the SHARP system [4] have reported that the coherent illumination exhibits field-dependent angular variations, caused by a relative defocus between the illumination and the object planes. To address this issue, we apply a first-order approximation and conduct a grid search over the parameter α:

$$\overrightarrow{k_t} = \overrightarrow{k_0} + \alpha \cdot \overrightarrow{x_t} \tag{2}$$

where $\overrightarrow{k_t}$ is the field dependent illumination vector at position $\overrightarrow{x_t}$, and $\overrightarrow{k_0}$ is the central illumination vector.

Fig. 5 illustrates the effectiveness of this correction by showing the corner patch reconstructed with the GN algorithm. Post-correction improvements are evident as the central dots become better resolved. Additionally, there is a noticeable overall lift of the FRC plot between the reconstruction and the central 'ground truth', as discussed in Sec. 4.2.

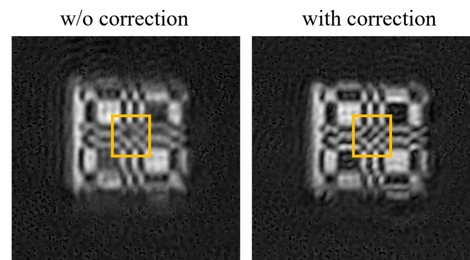

Fig. 5. Improvement in reconstruction quality after systematic illumination error correction, demonstrating enhanced image quality in the corner patch.

Authorized licensed use limited to: Lawrence Berkeley National Laboratory. Downloaded on January 14,2025 at 19:04:13 UTC from IEEE Xplore. Restrictions apply.

5. REFERENCES

[1] Guoan Zheng, Roarke Horstmeyer, and Changhuei Yang, "Wide-field, high-resolution fourier ptychographic microscopy," *Nature photonics*, vol. 7, no. 9, pp. 739–745, 2013.

[2] Antoine Wojdyla, Markus P. Benk, Patrick P. Naulleau, and Kenneth A. Goldberg, "Euv photolithography mask inspection using fourier ptychography," *Proceeedings of SPIE 10656, 106560W*, 2018.

[3] Kenneth A Goldberg, Iacopo Mochi, Markus Benk, Arnaud P Allezy, Michael R Dickinson, Carl W Cork, Daniel Zehm, James B Macdougall, Erik Anderson, Farhad Salmassi, et al., "Commissioning an euv mask microscope for lithography generations reaching 8 nm," in *Extreme Ultraviolet (EUV) Lithography IV*. SPIE, 2013, vol. 8679, pp. 347–356.

[4] Gautam Gunjala, Antoine Wojdyla, Stuart Sherwin, Aamod Shanker, Markus P Benk, Kenneth A Goldberg, Patrick P Naulleau, and Laura Waller, "Extreme ultraviolet microscope characterization using photomask surface roughness," *Scientific reports*, vol. 10, no. 1, pp. 11673, 2020.

[5] Xiaoze Ou, Guoan Zheng, and Changhuei Yang, "Embedded pupil function recovery for fourier ptychographic microscopy," *Optics express*, vol. 22, no. 5, pp. 4960–4972, 2014.

[6] Lei Tian, Xiao Li, Kannan Ramchandran, and Laura Waller, "Multiplexed coded illumination for fourier ptychography with an led array microscope," *Biomedical optics express*, vol. 5, no. 7, pp. 2376–2389, 2014.

[7] Ruizhi Cao, Cheng Shen, and Changhuei Yang, "High-resolution, large field-of-view label-free imaging via aberration-corrected, closed-form complex field reconstruction," *arXiv preprint arXiv:2309.00755*, 2023.

[8] Pengming Song, Shaowei Jiang, He Zhang, Xizhi Huang, Yongbing Zhang, and Guoan Zheng, "Full-field fourier ptychography (ffp): Spatially varying pupil modeling and its application for rapid field-dependent aberration metrology," *APL Photonics*, vol. 4, no. 5, 2019.

[9] Li-Hao Yeh, Jonathan Dong, Jingshan Zhong, Lei Tian, Michael Chen, Gongguo Tang, Mahdi Soltanolkotabi, and Laura Waller, "Experimental robustness of fourier ptychography phase retrieval algorithms," *Optics express*, vol. 23, no. 26, pp. 33214–33240, 2015.

[10] Niccolo Banterle, Khanh Huy Bui, Edward A Lemke, and Martin Beck, "Fourier ring correlation as a resolution criterion for super-resolution microscopy," *Journal of structural biology*, vol. 183, no. 3, pp. 363–367, 2013.

Authorized licensed use limited to: Lawrence Berkeley National Laboratory. Downloaded on January 14,2025 at 19:04:13 UTC from IEEE Xplore. Restrictions apply.